Microscopic simulation of a strongly coupled hydrogen plasma

J. P. Hansen
Laboratoire de Physique Théorique des Liquides, Université Pierre et Marie Curie, 4 Place Jussieu, 75230 Paris Cedex 05, France

I. R. McDonald
Department of Physical Chemistry, University of Cambridge, Lensfield Road, Cambridge, United Kingdom

(Received 28 April 1980)

Results of "molecular dynamics" simulations are reported for a model of a fully ionized strongly coupled hydrogen plasma. Quantum effects are taken into account through the use of effective pair potentials; at short distances, these differ significantly from the bare Coulomb potential. Static properties of the plasma are shown to be well described by hypernetted chain theory. The ion- and electron-velocity autocorrelation functions have been computed and the electrical conductivity turns out to be roughly twice that expected on the basis of the electron self-diffusion coefficient. The predictions of Vlasov theory for the damping and dispersion of the plasmon mode are found to be in generally poor agreement with the results of the computer "experiments", but the collective dynamical properties are successfully described by a memory-function scheme in which explicit account is taken of ion-electron correlations. Prospects for future work are briefly reviewed.

I. INTRODUCTION

Models of highly compressed plasmas corresponding to electron densities of order 10^{24} cm^{-3} or more are of considerable interest because of their relevance to the study of matter under extreme conditions, particularly those encountered in astrophysical problems and in inertial confinement experiments.[1,2] Under such conditions, the mean kinetic and potential energies of particles in the plasma are typically of the same order of magnitude, and the plasma is said to be *strongly correlated* or *strongly coupled*. The microscopic dynamics of ions and electrons in a strongly coupled plasma are dominated by collisions and standard kinetic theoretical treatments[3] based, for example, on the Vlasov approximation are inapplicable. At the same time, because the collision rate is high, a strongly coupled plasma approaches thermodynamic equilibrium much more rapidly than in the low-density case, so that the study of equilibrium properties becomes of greater physical significance.

In attempting to characterize the thermodynamic state of a strongly coupled plasma, it is possible to distinguish between two quite different regimes of density and temperature. Let $n = N/V$ be the number of ions of charge Ze per unit volume; the corresponding electron number density is nZ. A convenient scale of length is the "ion sphere" radius a defined by

$$a^3 = 3/4\pi n . \tag{1}$$

If m_e is the electron rest mass, the Fermi degeneracy temperature is

$$T_F = \frac{\hbar^2 (3\pi^2 nZ)^{2/3}}{2m_e k_B} . \tag{2}$$

Provided the electron density is sufficiently high for T_F to be much greater than the temperature of the plasma, the electrons form a degenerate Fermi gas. The latter may be treated independently of the ionic fluid if the Thomas-Fermi screening length λ_{TF} exceeds the mean interionic spacing as measured by the quantity a, i.e., if

$$\lambda_{TF} = \left(\frac{\pi}{3n}\right)^{1/6} \frac{\hbar}{2Ze m_e^{1/2}} > a . \tag{3}$$

Apart from ionic quantum corrections, which are important only at extremely low temperatures, the system is then reasonably well described as a classical "one-component plasma" (OCP), in which the degenerate electron gas plays the role of a uniform neutralizing background. The static and dynamic properties of the OCP have been extensively studied over the past decade and can, by now, be considered as well known.[4]

This paper is concerned with the opposite regime, in which the temperature is of the order of T_F, or higher. The electron gas is now nondegenerate and the plasma may be treated as an almost classical two-component fluid the "two-component plasma" (TCP). In the TCP, quantum diffraction and symmetry effects become significant only when two particles approach each other closer than the de Broglie thermal wavelength. Such effects can be handled by the use of effective pair potentials. These differ from the bare Coulomb potentials only at short distances, but prevent the collapse characteristic of purely classical systems of particles of opposite charge.

The present work is restricted to the study of a fully ionized nearly classical hydrogen plasma made up of equal numbers of protons ($Z = 1$) and electrons. The "experimental" basis of the work

is provided by the results of microscopic simulations carried out by the method of "molecular dynamics" (MD), a technique borrowed from the field of classical liquids.[5] Simulations have been performed for three thermodynamic states of the model plasma described in Sec. II. Results for the static properties are analyzed in Sec. III; the self-diffusion of the electrons and protons and the electrical conductivity of the plasma are discussed in Sec. IV; Sec. V is devoted to the results obtained for the longitudinal collective motions, primarily to the charge-fluctuation (plasmon) modes. The collective modes are further analyzed in Sec. VI in the framework of a memory-function approach which takes explicit account of the coupling between the microscopic partial densities of the two charged species. Some concluding remarks and prospects for future work are contained in Sec. VII. A preliminary account of parts of this work has been published elsewhere.[6]

II. THE MODEL

An equilibrium state of the plasma we have just described is fully characterized by two independent thermodynamic variables. Obvious choices include the temperature T and the ion (or electron) number density n. It is more convenient, however, to work with dimensionless variables. To that end, we define a *coupling constant* or *plasma parameter* Γ as

$$\Gamma = l/a , \tag{4}$$

where

$$l = e^2/k_B T \tag{5}$$

is the Landau length, and introduce a dimensionless length parameter r_S by taking the ratio of the ion-sphere radius to the Bohr radius a_0, i.e.,

$$r_S = \frac{a}{a_0} = \frac{a m_e e^2}{\hbar^2} . \tag{6}$$

Note that if n is measured in A^{-3}, its numerical value is $1.61/r_S^3$.

The coupling constant Γ is roughly the ratio of the mean potential energy of a pair of neighboring ions (or electrons) to the mean kinetic energy of a particle in the plasma. Low-density plasmas are those for which $\Gamma \ll 1$, whereas in the present work we are interested in the strong coupling regime, i.e., $\Gamma \sim 1$.

Another length parameter is the Debye-screening length Λ_D, where

$$\Lambda_D^{-2} = \frac{8\pi n e^2}{k_B T} \tag{7}$$

and an alternative choice[3] of plasma parameter is the quantity ϵ defined as

$$\epsilon = \frac{4\pi e^2}{\Lambda_D k_B T} = 4\pi\sqrt{6}\,\Gamma^{3/2} . \tag{8}$$

In order to understand the physical significance of the parameter ϵ it is sufficient to note that the mean number of particles in a Debye cube is $2n\Lambda_D^3$, i.e., ϵ^{-1}. It follows that the concept of a Debye-screening length loses its meaning in the strong coupling regime, since in that case the number ϵ^{-1} is less than one. Under such conditions, the assumptions underlying the mean field approach typified by the Vlasov approximation (or its static analog, the Debye-Hückel theory) cease to have any validity.

A measure of the importance of quantum effects for either ions or electrons is given by the ratios of the corresponding de Broglie thermal wavelengths, i.e.,

$$\lambda\!\!\!^{-}_i = \frac{\hbar}{(2\pi m_i k_B T)^{1/2}} , \quad \lambda\!\!\!^{-}_e = \frac{\hbar}{(2\pi m_e k_B T)^{1/2}} , \tag{9}$$

to the ion-sphere radius. Ionic quantum corrections are in general completely negligible ($\lambda\!\!\!^{-}_i/a \ll 1$), but the very low mass of the electron means that electronic quantum effects remain important up to relatively high temperatures. It is well known[7] that inclusion of quantum-diffraction effects and electron Fermi statistics is essential in order to guarantee the thermodynamic stability of a plasma. In the nondegenerate electron gas, however, quantum effects come into play only for pair separations which are small compared to a, since $\lambda\!\!\!^{-}_e/a < 1$ for $T/T_F \gtrsim 1$. Note that

$$\left(\frac{\lambda\!\!\!^{-}_e}{a}\right)^2 = \frac{1}{\pi}\left(\frac{4}{9\pi}\right)^{2/3}\frac{T_F}{T} = \frac{1}{2\pi}\frac{\Gamma}{r_S} . \tag{10}$$

The condition $\lambda\!\!\!^{-}_e < a$ therefore imposes a restriction on the values which can be taken simultaneously by Γ and r_s.

In order to treat the nondegenerate hydrogen plasma by classical statistical mechanics, use is made of *effective* pair potentials, which account for diffraction and symmetry effects in an approximate way. Effective pair potentials may be derived by expressing the quantum-mechanical Slater sum

$$W(\{\vec{r}_i\}) = \sum_n \psi_n^* \exp(-\beta E_n)\psi_n \tag{11}$$

in a form reminiscent of the classical Boltzmann factor,[8] i.e., as

$$W \simeq \exp\left(-\beta \sum_{i<j} v(i,j)\right) . \tag{12}$$

In Eq. (11), ψ_n and E_n are the eigenfunctions and

eigenvalues of the full Hamiltonian of the system, $\{\vec{r}_i\}$ denotes the set of all position vectors of the N electrons and N protons of the plasma, and $v(i,j)$ represents the effective pair potential between particles i and j. In the classical (high-temperature) limit, $v(i,j)$ must reduce to the bare Coulomb potential between the two particles, i.e.,

$$\lim_{T\to\infty} v(i,j) = \frac{\epsilon_i \epsilon_j e^2}{|\vec{r}_i - \vec{r}_j|}, \tag{13}$$

where $\epsilon_i, \epsilon_j = +1$ (ions), or -1 (electrons). An effective potential determined in this way is usually dependent both on temperature and density. Effective pair potentials appropriate to the low-density limit have been derived for the hydrogen plasma by Barker[9] and by Deutsch and collaborators[10,11] from an exact numerical computation of the two-particle Slater sum for electron-electron and electron-proton pairs. At sufficiently high temperatures ($k_B T > 1$ Ry), the contribution of bound states to the electron-proton Slater sum can be neglected. If, moreover, the scattering states are limited to s waves, and if symmetry effects are neglected for electron-electron pairs, the following very simple effective potentials can be derived[10]:

$$v_{\alpha\beta}(r) = \frac{\epsilon_\alpha \epsilon_\beta e^2}{r}\left[1 - \exp\left(\frac{-r}{\lambda\!\!\!^{-}_{\alpha\beta}}\right)\right], \tag{14}$$

with $\alpha, \beta = i$ (ions), e (electrons), and

$$\lambda\!\!\!^{-}_{\alpha\beta} = \frac{\hbar}{(2\pi\mu_{\alpha\beta} k_B T)^{1/2}}, \tag{15}$$

where $\mu_{\alpha\beta} = (m_\alpha^{-1} + m_\beta^{-1})^{-1}$ is the reduced mass of an α-β pair. The fact that the potentials $v_{\alpha\beta}(r)$ remain finite as $r \to 0$ is a consequence of the uncertainty principle and prevents the collapse to which we have already referred. At the temperatures of interest $\lambda\!\!\!^{-}_{ii} \ll a$. Thus the effective ion-ion interaction is virtually identical to the bare Coulomb potential at all separations.

To take account of symmetry effects (i.e., the Pauli principle) for the electrons, a term must be added to the effective electron-electron potential. It has been shown[11] that in the high-temperature limit

$$\begin{aligned} v_{ee}(r) &= v_{ee}^{(d)}(r) + v_{ee}^{(s)}(r) \\ &= \frac{e^2}{r}\left[1 - \exp\left(\frac{-r}{\lambda\!\!\!^{-}_{ee}}\right)\right] \\ &\quad + k_B T (\ln 2) \exp\left(\frac{-r^2}{\pi \lambda\!\!\!^{-2}_{ee} (\ln 2)}\right), \end{aligned} \tag{16}$$

where the first term $v_{ee}^{(d)}(r)$ arises from quantum-diffraction effects, while the second $v_{ee}^{(s)}(r)$ takes care of symmetry. Note that $\lambda\!\!\!^{-}_{ee} = \sqrt{2}\,\lambda\!\!\!^{-}_{e}$, and for infinitely heavy ions ($m_i/m_e \to \infty$), $\lambda\!\!\!^{-}_{ie} \to \lambda\!\!\!^{-}_{e}$, and $\lambda\!\!\!^{-}_{ii} \to 0$.

An important approximation made throughout this paper is the neglect of the density dependence of the effective pair potentials, even at electron densities of order 10^{24} cm^{-3}. We believe this to be a reasonable approximation so long as $\lambda\!\!\!^{-}_{\alpha\beta}/a \ll 1$, i.e., for a sufficiently nondegenerate plasma, since there are some theoretical indications[8] that the density dependence of the $v_{\alpha\beta}(r)$ is indeed weak. We have also implicitly assumed that the effective potential for clusters of three or more particles is pairwise additive. The reason for restricting the calculations to the simplest set of effective potentials lies in our special interest in the collective dynamical modes of the plasma: We assume the character of these to be dictated primarily by the long range of the potential and therefore insensitive to details of the behavior at short range. For the same reason, the numerical simulations have been carried out with the pair potentials defined in Eq. (14), i.e., *without* the symmetry part $v_{ee}^{(s)}(r)$ of the electron-electron potential. It will become clear from the theoretical analysis given in Sec. VI that the collective dynamics are largely unaffected by this simplification. In order to avoid the difficult problems associated with ionization equilibrium,[12] our calculations have been restricted to temperatures of order 1 Ry (160 000 K) or higher. Figure 1 shows the region of the n-T plane of interest in the present work, i.e., that corresponding to a nondegenerate fully ionized and strongly coupled hydrogen plasma.

In our MD calculations, we have simulated a system consisting of 125 protons and 125 electrons for the three thermodynamic states indicated in

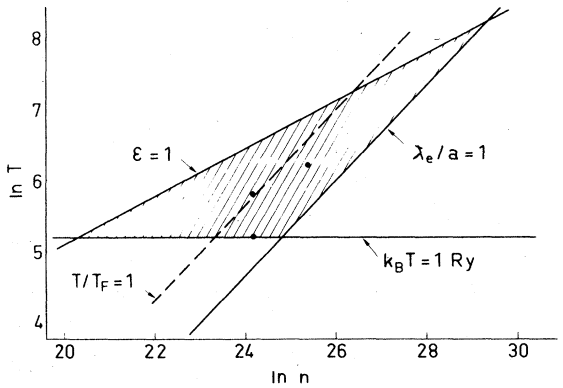

FIG. 1. Part of the density-temperature plane; n is in cm^{-3} and T is in kelvin. The shaded area represents the region of approximate validity of the models described in the text. The dots denote the thermodynamic states for which MD calculations have been made.

Fig. 1 and Table I; similar calculations have already proved to be of value in the study both of the OCP (Refs. 13 and 14) and of binary ionic mixtures.[15] Note that the condition $\chi_e < a$ is satisfied in all three cases whereas the condition $T > T_F$ is satisfied only for $\Gamma = 0.5$, $r_s = 1$. Clearly the approximations underlying the use of Eqs. (14) and (16) are poorest for the case $\Gamma = 2$, $r_s = 1$.

A natural time scale in a MD simulation is the inverse of the electron plasma frequency ω_{pe}, defined as

$$\omega_{pe} = (4\pi n e^2/m_e)^{1/2} . \tag{17}$$

The coupled equations of motion for the 250 particles in the system were integrated numerically by a standard finite difference algorithm with a time increment Δt which is given for each run in Table I. The time increment was chosen to be as large as possible subject to an acceptable degree of conservation of the total energy and of the total linear momentum of the system. Periodic boundary conditions were used throughout and the total force acting on a given particle from all other particles in the basic cell, as well as from the infinite array of their periodic images, was summed according to a standard Ewald procedure.[13,16] The total number of time steps generated for each of the three thermodynamic states is shown in Table I. It should be noted that in practice each of the runs was broken up into two parts of comparable length, and that overall averages were taken over the total length of the two parts.

A potential source of difficulty in such a simulation is the large difference in time scales of the electronic and ionic motions. The microscopic dynamics scale roughly as the inverse of the electron- and ion-plasma frequencies, ω_{pe} and ω_{pi}, i.e., as the square root of the masses. [Note that ω_{pi} is defined analogously to ω_{pe}, Eq. (17).] Thus the time scale of the protons exceeds that of the electrons by a factor of approximately $(m_i/m_e)^{1/2} (\simeq 43)$, the choice of Δt being dictated by the *electronic* motion. Each of our runs covers several thousand electron plasma oscillations, but only of order 100 ion-plasma oscillations; the statistics on the electronic motion are therefore correspondingly greater. However, despite the large ion-to-electron mass ratio, we experienced no particular difficulty in either reaching or maintaining thermal equilibrium.

TABLE I. Details of the molecular-dynamics calculations. Δt is the time step in the numerical integration and N_t is the total number of steps in the simulation.

Γ	0.5	0.5	2
r_S	0.4	1	1
T(K)	1.58×10^6	6.32×10^5	1.58×10^5
n(cm^{-3})	2.5×10^{25}	1.6×10^{24}	1.6×10^{24}
ω_{pe}(s^{-1})	2.8×10^{17}	7.2×10^{16}	7.2×10^{16}
$\omega_{pe}\Delta t$	0.03	0.03	0.08
N_t	5.6×10^4	7.3×10^4	4.8×10^4

Finally, it is useful to contrast the present MD calculations with more standard simulations of one- and two-dimensional plasmas, namely, those based on a calculation of the forces from a numerical solution to Poisson's equation on a grid of finite mesh size.[17] The latter technique is well suited for nearly collisionless plasmas, since close encounters between particles are not treated correctly; it allows the simulation of relatively large systems ($N \sim 10^4$ particles) in the weak-coupling limit (many particles in a Debye cube), and has been applied successfully in recent years to the study of plasma turbulence. The present technique, on the other hand, is complementary to the former, since it is particularly efficient for the simulation of strongly coupled plasmas in or near, thermodynamic equilibrium. Since the number of particles in a Debye cube is of order one, or less, the simulated system need not be so large as in the previous calculations. The extension to nonequilibrium situations appears to be feasible, and work in that direction is in progress.

III. STATIC PROPERTIES

The static structural information which we have extracted from the simulations is contained in the three partial pair distribution functions $g_{ii}(r)$, $g_{ie}(r)$, and $g_{ee}(r)$. We should stress from the outset that the computation of static quantities was not the primary goal of the present work. Had we been interested only in time-independent statistical averages, it would have been much more efficient either to simulate a hypothetical plasma in which ions and electrons have the same mass or to use a Monte Carlo method. In fact, we ran one equal mass simulation at $\Gamma = 0.5$, $r_s = 0.4$, which allowed us to compute $g_{ii}(r)$ with considerably more accuracy than in the three runs listed in Table I. Since the effective potentials are assumed to be pairwise additive, knowledge of the pair distribution functions is sufficient to determine both the pressure P and excess internal energy U. Thus

$$\frac{P}{2nk_BT} = 1 - \tfrac{1}{3}\pi n \sum_\alpha \sum_\beta \int_0^\infty g_{\alpha\beta}(r) \frac{dv_{\alpha\beta}(r)}{dr} r^3 \, dr , \tag{18}$$

$$\frac{U}{2N} = \pi n \sum_\alpha \sum_\beta \int_0^\infty g_{\alpha\beta}(r) \left(v_{\alpha\beta}(r) - T \frac{\partial}{\partial T} v_{\alpha\beta}(r) \right) r^2 dr . \tag{19}$$

Note that Eq. (19) differs from the usual expression[5] for the internal energy by terms related to the temperature dependence of the effective potentials (14) and (16).

The partial structure factors of the system are defined as the static (equal-time) correlation functions of the Fourier components of the microscopic partial densities, i.e., as

$$S_{\alpha\beta}(k)=\frac{1}{N}\langle\rho^{(\alpha)}(\vec{k})\rho^{(\beta)}(-\vec{k})\rangle\,, \tag{20}$$

where α, $\beta=i$, e and

$$\rho^{(\alpha)}(\vec{k})=\sum_{i=1}^{N}\exp(i\vec{k}\cdot\vec{r}_i^{(\alpha)})\,. \tag{21}$$

They are related to the Fourier transforms of the pair correlation functions $h_{\alpha\beta}(r)=g_{\alpha\beta}(r)-1$ by

$$\begin{aligned}S_{\alpha\beta}(k)&=\delta_{\alpha\beta}+\hat{h}_{\alpha\beta}(k)\\&=\delta_{\alpha\beta}+4\pi n\int_0^\infty\frac{\sin kr}{kr}h_{\alpha\beta}(r)r^2\,dr\,.\end{aligned} \tag{22}$$

A linear combination of the partial structure factors which is of particular importance is the charge structure factor, defined as

$$\begin{aligned}S_{zz}(k)&=\frac{1}{2N}\langle\rho^z(\vec{k})\rho^z(-\vec{k})\rangle\\&=\tfrac{1}{2}[S_{ii}(k)+S_{ee}(k)-2S_{ie}(k)]\,,\end{aligned} \tag{23}$$

where

$$\rho^z(\vec{k})=\rho^{(i)}(\vec{k})-\rho^{(e)}(\vec{k})\,. \tag{24}$$

The long-wavelength limit of the partial structure factors is related[18] to the isothermal compressibility by

$$\lim_{k\to0}S_{\alpha\beta}(k)=nk_BT\chi_T=k_BT\left(\frac{\partial P}{\partial n}\bigg|_T\right)^{-1}, \tag{25}$$

while the charge neutrality and perfect screening conditions imply[18,19] that

$$\lim_{k\to0}\frac{k_D^2}{k^2}S_{zz}(k)=1\,, \tag{26}$$

where $k_D=1/\Lambda_D$ is the inverse of the Debye length (7), often called the Debye wave number.

The static dielectric function $\epsilon(k)$ is directly related to the charge structure factor by the fluctuation-dissipation theorem[20] in the form

$$\frac{1}{\epsilon(k)}=1-\frac{k_D^2}{k^2}S_{zz}(k)\,. \tag{27}$$

Note that in the weak coupling (Debye-Hückel) limit

$$\lim_{\Gamma\to0}\frac{1}{\epsilon(k)}=\lim_{\Gamma\to0}S_{zz}(k)=\frac{k^2}{k^2+k_D^2}\,. \tag{28}$$

Among the usual approximate integral equations for the pair distribution functions of fluids, the most successful for ionic systems is the so-called hypernetted chain (HNC) equation.[4,5] For the binary system of interest here, the HNC approximation for the three pair distribution functions may be written as

$$g_{\alpha\beta}(r)=\exp[-\beta v_{\alpha\beta}(r)+h_{\alpha\beta}(r)-c_{\alpha\beta}(r)]\,, \tag{29}$$

which supplements the three coupled Ornstein-Zernike defining relations for the direct correlation functions $c_{\alpha\beta}(r)$. In $\vec{k}$ space, the Ornstein-Zernike relations take the form

$$\hat{h}_{\alpha\beta}(k)=\hat{c}_{\alpha\beta}(k)+\sum_\gamma\hat{h}_{\alpha\gamma}(k)\hat{c}_{\gamma\beta}(k)\,, \tag{30}$$

$$\hat{c}_{\alpha\beta}(k)=4\pi n\int_0^\infty\frac{\sin kr}{kr}c(r)r^2dr\,. \tag{31}$$

We have solved the coupled Eqs. (29), (30), and (31) numerically for several thermodynamic states by a standard iterative procedure. Since the $c_{\alpha\beta}(r)$ behave like $-\beta v_{\alpha\beta}(r)$ for large r, their Fourier transforms are singular ($\sim k^{-2}$) in the $k\to0$ limit, and some care is needed if numerical errors are to be avoided. In the present work, we have adapted to the two-component case, the procedure developed by Springer *et al.*[21] and Ng[22] for the OCP. We find that for $\Gamma\simeq1$, excellent

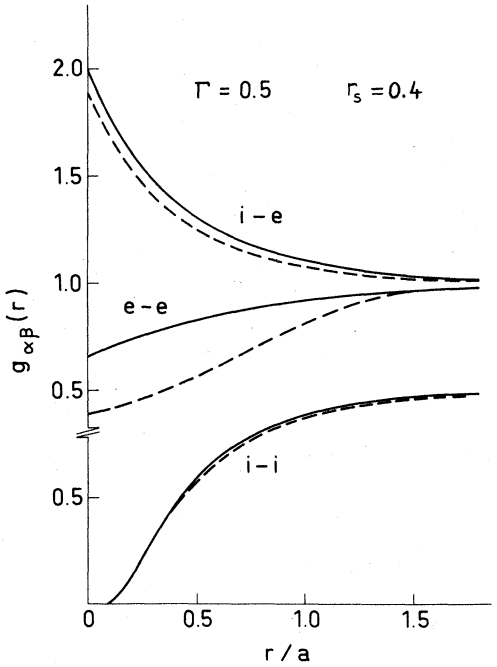

FIG. 2. HNC results for partial pair distribution functions. Full curves: Based on the potential model defined by Eq. (14). Dash curves: Based on potential model which incorporates electron symmetry, defined by Eq. (16).

TABLE II. Thermodynamic properties. MD: molecular-dynamics results; HNC(1): results of HNC calculations based on potential model defined by Eq. (14); HNC(2): results of HNC calculations based on potential model incorporating electron symmetry defined by Eq. (16).

		$\frac{PV}{2Nk_BT}$			$\frac{U}{2Nk_BT}$		$2nk_BT\chi_T$	
Γ	r_S	MD	HNC(1)	HNC(2)	HNC(1)	HNC(2)	HNC(1)	HNC(2)
0.5	0.4	0.91	0.940	1.394	−0.206	+0.044	1.082	0.788
0.5	1	0.89	0.928	0.966	−0.243	−0.187	1.101	1.012
2	1	0.63	0.737	1.089	−0.962	−0.435	0.754	0.728

numerical convergence is obtained with very few (~10) iterations. The three resulting pair distribution functions are shown in Fig. 2 for $\Gamma = 0.5$ and $r_S = 0.4$. The qualitative features of the $g_{\alpha\beta}(r)$ are as expected, and the agreement between the "exact" MD data and HNC results is excellent; similarly good agreement is observed for the other thermodynamic states (see, in particular, Fig. 1 of Ref. 6).

Figure 2 also illustrates the influence of the Pauli exclusion principle on the three $g_{\alpha\beta}(r)$. When electron symmetry effects [represented by the term $v_{ee}^{(s)}(r)$ in Eq. (16)] are included in the effective electron-electron potential, $g_{ee}(r)$ is considerably depleted at short distances. In particular, the obvious inequality $g_{ee}(r=0) \leq \frac{1}{2}$ is violated when $v_{ee}^{(s)}(r)$ is omitted, but is automatically satisfied, at least in the low-density limit, when it is included. The other pair distribution functions $g_{ii}(r)$ and $g_{ie}(r)$ are much less sensitive to electron symmetry considerations.

In Table II we compare selected thermodynamic data from the MD simulations with the results of HNC calculations for three thermodynamic states. The HNC results have been obtained both with and without the incorporation of symmetry; as is to be expected, the additional repulsion between electrons arising from the Pauli principle has the effect of considerably increasing the pressure, especially at the lower temperature ($\Gamma = 2$). The equations of state along three isochores, as calculated from the HNC equations with the full effective electron-electron potential [Eq. (16)], are shown in Fig. 3. The ion-electron attraction manifests itself in a negative minimum of the excess compressibility factor $(P/2nk_BT - 1)$ as a function of coupling (or inverse temperature) at the two lower densities. In Fig. 4 we show the in-

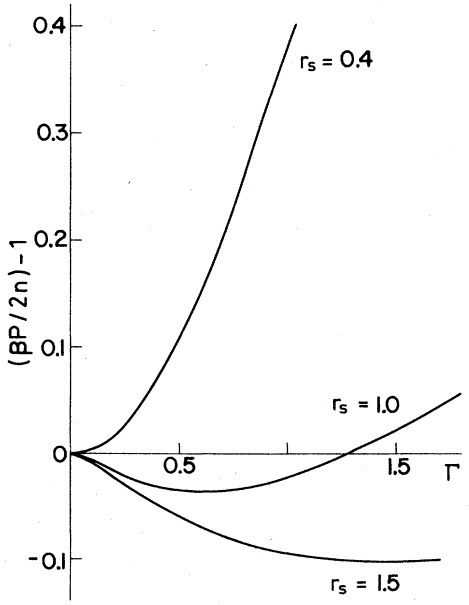

FIG. 3. HNC results for the equation of state for the model which incorporates electron symmetry, defined by Eq. (16).

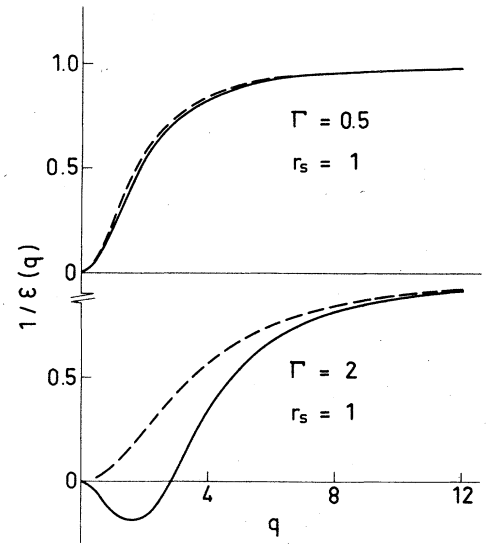

FIG. 4. Inverse static dielectric function for $r_S = 1$, $\Gamma = 0.5$ (above) and $\Gamma = 2$ (below). Full curves: HNC results for the potential model which incorporates electron symmetry, defined by Eq. (16). Dash curves: Debye-Hückel approximation.

verse static dielectric function $1/\epsilon(k)$ as a function of the reduced wave number $q = ak$ for $r_S = 1$, $\Gamma = 0.5$ and 2. The HNC results (which are virtually indistinguishable from the MD data) are compared in Fig. 4 with the predictions of mean-field (i.e., Debye-Hückel) theory embodied in Eq. (27). The breakdown of mean-field theory is particularly evident at $\Gamma = 2$ where, as a consequence of the strong correlations between particles, $\epsilon(k)$ exhibits a negative region for $q < 3$.

IV. SELF-DIFFUSION AND ELECTRICAL CONDUCTIVITY

The self-diffusion of both ions and electrons has been studied by computing the corresponding normalized velocity autocorrelation functions (ACF's), defined as

$$Z_\alpha(t) = \frac{\langle \vec{v}^{(\alpha)}(t) \cdot \vec{v}^{(\alpha)}(0) \rangle}{\langle |\vec{v}^{(\alpha)}|^2 \rangle}, \tag{32}$$

where $\vec{v}^{(\alpha)}(t)$ is the velocity at time t of a given ion ($\alpha = i$) or electron ($\alpha = e$). The MD results for $Z_e(t)$ at $\Gamma = 0.5$ and $r_S = 0.4$ and 1 are shown in Fig. 5 and results for both $Z_i(t)$ and $Z_e(t)$ at $\Gamma = 2$, $r_S = 1$ can be found in Fig. 2 of Ref. 6. The two diffusion coefficients D_e and D_i are then obtained from the standard relation

$$D_\alpha = \frac{k_B T}{m_\alpha} \int_0^\infty Z_\alpha(t)\, dt \tag{33}$$

and results for the absolute and reduced ($D_\alpha^* = D_\alpha / a^2 \omega_{p\alpha}$) diffusion coefficients are listed in Table III. Although the statistics on $Z_i(t)$ are poor, it is clear that the functions $Z_i(t)$ and $Z_e(t)$ are almost identical when plotted on the appropriate reduced time scale ($t^* = \omega_{p\alpha} t$); the two reduced diffusion coefficients are therefore approximately the same for given values of Γ and r_S. The best

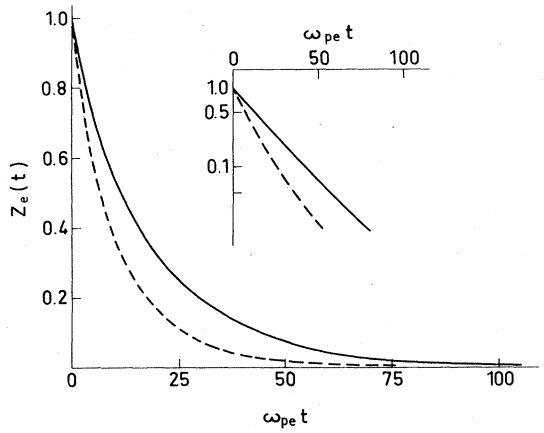

FIG. 5. Electron velocity ACF for $\Gamma = 0.5$, $r_S = 0.4$ (full curves) and $r_S = 1$ (dash curves).

statistics on the ionic motion are those obtained for the state point $\Gamma = 2$, $r_S = 1$. In that case it is found that $Z_i(t^*)$ decays somewhat faster than $Z_e(t^*)$ at large times,[6] and D_i^* is in consequence some 20 to 25% smaller than D_e^*. It should be noted that neither of the two velocity ACF's exhibits any oscillatory behavior of the type observed, under conditions of stronger coupling ($\Gamma \gtrsim 10$), in MD simulations[13] of the OCP. Instead, the decay is roughly exponential, as can be seen from the inset to Fig. 5.

The electrical conductivity per unit volume σ, can be determined from the time integral of the electrical current ACF $J(t)$, by the standard Green-Kubo formula[5]

$$\sigma = \frac{\omega_p^2}{4\pi} \int_0^\infty J(t)\, dt, \tag{34}$$

where $\omega_p^2 = \omega_{pi}^2 + \omega_{pe}^2$ is the square of the total plasma frequency (note that $\omega_p \simeq \omega_{pe}$). The normalized ACF $J(t)$ is defined as

$$J(t) = \frac{\langle \vec{j}(t) \cdot \vec{j}(0) \rangle}{\langle |\vec{j}|^2 \rangle}, \tag{35}$$

with

$$\vec{j}(t) = \vec{j}_i(t) - \vec{j}_e(t), \tag{36}$$

where

$$\vec{j}_\alpha(t) = \sum_{i=1}^{N} \vec{v}_i^{(\alpha)}(t). \tag{37}$$

Since the total linear momentum is conserved, i.e.,

$$\vec{P}(t) = m_i \vec{j}_i(t) + m_e \vec{j}_e(t) = \vec{P}(0) \tag{38}$$

it follows that $J(t)$ can also be written as

$$J(t) = 1 - \frac{(m_i + m_e)}{3Nk_BT} \langle \vec{j}_e(t) \cdot \vec{j}_i(0) \rangle. \tag{39}$$

Since fluctuations in $\vec{j}_e(t)$ are much more rapid than those in $\vec{j}_i(t)$, it follows from Eq. (39) that $J(t)$ should decay on roughly the same timescale as $Z_e(t)$. This is true, as we have shown elsewhere[6] for the case $\Gamma = 2$, $r_S = 1$, but it is also a fact that the lifetime of $J(t)$ is significantly longer (by a factor of two or more) than that of $Z_e(t)$. We have found similar results at $\Gamma = 0.5$, $r_S = 0.4$ and 1, though in these two cases the runs were not of sufficient length to yield reliable values for the conductivity.

If the correlation between the velocities of different particles were negligible at all times, the electrical conductivity could be determined from the self-diffusion constants of the two species by applying a relation of the Nernst-Einstein form,

TABLE III. Results for self-diffusion coefficients and electrical conductivity. Starred quantities are in units in which $\omega_{pe}=a=1$ and either $\omega_{pi}=1$ (for D_i^*, τ_{si}^*, and ω_{si}^*) or $\omega_{pe}=1$ (for other starred quantities).

	$\Gamma=0.5,\ r_S=0.4$	$\Gamma=0.5,\ r_S=1$	$\Gamma=2,\ r_S=1$
D_e^*	12.3 [a]	7.2 [a]	1.23 [a]
$D_e(\mathrm{cm^2\,s^{-1}})$	15.7 [a]	14.5 [a]	2.47 [a]
τ_{se}^*	0.489	0.349	0.910
ω_{se}^*	0.333	0.515	0.409
D_i^*			1.01 [a]
$D_i(\mathrm{cm^2\,s^{-1}})$			0.047 [a]
τ_{si}^*			0.36
ω_{si}^*	0.643	0.732	0.686
σ^*	3.6	2.15	1.1 [a]
$\sigma(\mathrm{mho\,cm^{-1}})$	17.2×10^5	1.7×10^5	0.9×10^5 [a]
τ_J^*	0.274	0.182	0.60
ω_J^*	0.284	0.451	0.370

[a] Results of molecular-dynamics calculations; other results obtained in the manner explained in the text.

namely,

$$\sigma=\frac{ne^2}{k_BT}(D_i+D_e), \tag{40}$$

or

$$\sigma^*=\frac{\sigma}{\omega_{pe}}=\frac{3\Gamma}{4\pi}\left[\left(\frac{m_e}{m_i}\right)^{1/2}D_i^*+D_e^*\right]. \tag{41}$$

The slow decay of $J(t)$ relative to that of $Z_e(t)$ means that the true conductivity is considerably larger than the estimate provided by Eq. (40). This contrasts with the situation found for molten salts, which may be regarded as "plasmas" consisting of ions of comparable mass and finite size, where the measured conductivity in a typical case has been found[23] to lie approximately 20% *below* the Nernst-Einstein value. Deviations from the Nernst-Einstein relation in molten salts may be explained in terms of short-lived positive correlations in the motion of neighboring ions of opposite charge, but the reasons for the behavior found for the plasma are at present unclear.

The two velocity ACF's may be expanded in power series about $t=0$. Thus

$$Z_\alpha(t)=1-\tfrac{1}{2}\omega_{s\alpha}^2t^2+O(t^4), \tag{42}$$

where

$$\omega_{s\alpha}^2=\frac{n}{3m_\alpha}\sum_{\beta=\alpha,\bar\alpha}\int_V g_{\alpha\beta}(r)\nabla^2v_{\alpha\beta}(r)\,d\vec r, \tag{43}$$

with $\alpha=i,e$ and $\bar\alpha(\neq\alpha)=e,i$. An exact representation of the two ACF's in terms of Fourier-Laplace transforms is obtained by writing

$$\tilde Z_\alpha(\omega)=\int_0^\infty e^{i\omega t}Z_\alpha(t)\,dt=\frac{1}{-i\omega+\tilde m_{s\alpha}^{(1)}(\omega)}, \tag{44}$$

where $\tilde m_{s\alpha}^{(1)}(\omega)$ is the transform of a first-order memory function $m_{s\alpha}^{(1)}(t)$. A single relaxation-time approximation for $m_{s\alpha}^{(1)}(t)$ which incorporates correctly the short-time expansion (42) is given by

$$m_{s\alpha}^{(1)}(t)=\omega_{s\alpha}^2\exp(-t^2/\tau_{s\alpha}^2) \tag{45}$$

or, equivalently, by

$$\tilde m_{s\alpha}^{(1)}(\omega)=\omega_{s\alpha}^2\tau_{s\alpha}[\Phi_1(\omega\tau_{s\alpha})+i\Phi_2(\omega\tau_{s\alpha})], \tag{46}$$

with

$$\Phi_1(x)=\tfrac{1}{2}\sqrt{\pi}\exp(-x^2/4), \tag{47}$$

$$\Phi_2(x)=\exp(-x^2/4)\int_0^{x/2}\exp(y^2)\,dy. \tag{48}$$

The relaxation time $\tau_{s\alpha}$ is related to the self-diffusion coefficient D_α by

$$D_\alpha=\frac{k_BT}{m_\alpha}\tilde Z(\omega=0)=\frac{k_BT}{m_\alpha}\frac{1}{\tilde m_{s\alpha}^{(1)}(\omega=0)}=\frac{k_BT}{m_\alpha}\frac{1}{\sqrt{\pi}\,\omega_{s\alpha}^2\tau_{s\alpha}}. \tag{49}$$

If we determine τ_{si} and τ_{se} by forcing agreement with the MD values of D_i and D_e, the resulting ACF's reproduce the results of the simulations to better than 5% over the whole range of t.

A similar analysis can be made of the electrical current ACF. The relevant short-time expansion is now

$$J(t) = 1 - \tfrac{1}{2}\omega_J^2 t^2 + O(t^4) \tag{50}$$

with

$$\omega_J^2 = \frac{n}{3}\frac{(m_i + m_e)}{m_i m_e}\int_V [g_{ie}(r) - 1]\nabla^2 v_{ie}(r)\, d\vec{r}\,. \tag{51}$$

If we approximate the first-order memory function in a manner similar to Eq. (45), the corresponding relaxation time τ_J turns out to be related to the electrical conductivity by the formula

$$\begin{aligned}\sigma &= \frac{\omega_p^2}{4\pi}\tilde{J}(\omega = 0) \\ &= \frac{\omega_p^2}{4\pi}\frac{1}{\tilde{m}_J^{(1)}(\omega = 0)} \\ &= \frac{\omega_p^2}{2\pi}\frac{1}{\sqrt{\pi}\,\omega_J^2 \tau_J}\,.\end{aligned} \tag{52}$$

By again imposing the MD value for the transport coefficient, a reasonable fit to the observed ACF is obtained in that case ($\Gamma = 2$, $r_S = 1$) for which reliable results on $J(t)$ are available out to large times. In the other two cases ($\Gamma = 0.5$, $r_S = 0.4$ and 1), we have inverted this procedure. That is to say, we have fitted the theoretical expression for $J(t)$ to the early part of the decay, i.e., down to $J(t) \simeq 0.3$, and have then extended the curves to large t in order to extract estimates for σ. The results, together with values for the other parameters entering both here and in the analysis of $Z_\alpha(t)$, are listed in Table III. The conductivities quoted in Table III differ markedly from the values given[24] by the formula of Spitzer, i.e.,

$$\sigma/(\text{mho cm}^{-1}) = \frac{1.53 \times 10^{-4}\, T^{3/2}}{\ln(\sqrt{3}\,\Gamma^{-3/2})} \tag{53}$$

where T is in kelvin. Indeed, at the lower temperature ($\Gamma = 2$), Eq. (53) predicts a negative conductivity. This breakdown of the formula is not unexpected, since it was derived under the condition $\Gamma \ll 1$.

V. COLLECTIVE LONGITUDINAL MODES

We now turn our attention to the wave-number dependence of the longitudinal collective motions of the ions and electrons. Let

$$\rho^{(\alpha)}(\vec{r}, t) = \sum_{i=1}^{N} \delta[\vec{r} - \vec{r}_i^{(\alpha)}(t)] \tag{54}$$

be the time-dependent microscopic density of species α; the Fourier components of the density are

$$\rho^{(\alpha)}(\vec{k}, t) = \sum_{i=1}^{N} \exp[i\vec{k}\cdot\vec{r}_i^{(\alpha)}(t)]\,. \tag{55}$$

We now define the three partial density-density time correlation functions as

$$F_{\alpha\beta}(k, t) = \frac{1}{N}\langle \rho^{(\alpha)}(\vec{k}, t)\rho^{(\beta)}(-\vec{k}, 0)\rangle\,. \tag{56}$$

As in the static case [see Eq. (20)], these are functions only of the length (as opposed to direction) of $\vec{k}$. Note also that $F_{ei}(k, t)$ and $F_{ie}(k, t)$ are identical. The corresponding dynamical structure factors are the Fourier transforms given by

$$S_{\alpha\beta}(k, \omega) = \frac{1}{2\pi}\int_{-\infty}^{+\infty} e^{i\omega t} F_{\alpha\beta}(k, t)\, dt\,. \tag{57}$$

Another set of correlation functions are those defined in terms of the dimensionless microscopic densities of mass and charge:

$$\rho^M(\vec{k}, t) = M\rho^{(i)}(\vec{k}, t) + \rho^{(e)}(\vec{k}, t)\,, \tag{58}$$

$$\rho^Z(\vec{k}, t) = \rho^{(i)}(\vec{k}, t) - \rho^{(e)}(\vec{k}, t)\,, \tag{59}$$

where $M = m_i/m_e \simeq 1836$ is the ion-to-electron mass ratio. (Thus we have arbitrarily chosen the electron rest mass as our mass unit.) The associated correlation functions are defined as

$$F_{ab}(k, t) = \frac{1}{2N}\langle \rho^a(\vec{k}, t)\rho^b(-\vec{k}, 0)\rangle\,, \tag{60}$$

where $a, b = M, Z$ and the corresponding dynamical structure factors are given by

$$S_{ab}(k, \omega) = \frac{1}{2\pi}\int_{-\infty}^{+\infty} e^{i\omega t} F_{ab}(k, t)\, dt\,. \tag{61}$$

The latter quantities are linear combinations of the partial dynamical structure factors. On writing out the relations explicitly, we find

$$S_{MM}(k, \omega) = \tfrac{1}{2}[M^2 S_{ii}(k, \omega) + 2MS_{ie}(k, \omega) + S_{ee}(k, \omega)]\,, \tag{62}$$

$$S_{MZ}(k, \omega) = \tfrac{1}{2}[MS_{ii}(k, \omega) + (1 - M)S_{ie}(k, \omega) - S_{ee}(k, \omega)]\,, \tag{63}$$

$$S_{ZZ}(k, \omega) = \tfrac{1}{2}[S_{ii}(k, \omega) - 2S_{ie}(k, \omega) + S_{ee}(k, \omega)]\,. \tag{64}$$

As is well known, the short-time expansion of any of the functions $F_{\alpha\beta}(k, t)$ is intimately related to the frequency moments of the corresponding dynamical structure factor. Thus,

$$\begin{aligned}(-1)^n F_{\alpha\beta}^{(2n)}(k, t = 0) &= \int_{-\infty}^{\infty} \omega^{2n} S_{\alpha\beta}(k, \omega)\, d\omega \\ &\equiv \Omega_{\alpha\beta}^{(2n)}\,,\end{aligned} \tag{65}$$

where $F_{\alpha\beta}^{(2n)}(k,t)$ is the $(2n)$th derivative with respect to t. The frequency moments are in turn expressible in terms of purely static properties. A straightforward calculation shows that

$$\Omega_{\alpha\beta}^{(0)}(k) = S_{\alpha\beta}(k), \tag{66}$$

$$\Omega_{\alpha\beta}^{(2)}(k) = \delta_{\alpha\beta}\frac{k_B T}{m_\alpha}k^2, \tag{67}$$

$$\Omega_{\alpha\beta}^{(4)}(k) = \frac{k_B T k^2}{(m_\alpha m_\beta)^{1/2}}\left(\frac{3k^2 k_B T}{m_\alpha}\delta_{\alpha\beta} + \delta_{\alpha\beta}\sum_\gamma \frac{K_{\alpha\gamma}}{m_\alpha} - \frac{1}{(m_\alpha m_\beta)^{1/2}}L_{\alpha\beta}(k)\right), \tag{68}$$

with

$$K_{\alpha\gamma} = \frac{n}{3}\int \nabla^2 v_{\alpha\gamma}(r) g_{\alpha\beta}(r)\, d\vec{r} = \frac{4\pi n}{3}\int_0^\infty \left(v''_{\alpha\gamma}(r) + \frac{2}{r}v'_{\alpha\gamma}(r)\right) g_{\alpha\beta}(r) r^2\, dr, \tag{69}$$

$$L_{\alpha\beta}(k) = n\int \exp(i\vec{k}\cdot\vec{r}) g_{\alpha\beta}(r)(\hat{k}\cdot\vec{\nabla})^2 v_{\alpha\beta}(r)\, d\vec{r} = 4\pi n\int_0^\infty \{v''_{\alpha\beta}(r)[(kr)^{-1}j_1(kr) - j_2(kr)] + (2/r)v'_{\alpha\beta}(r)(kr)^{-1}j_1(kr)\} g_{\alpha\beta}(r) r^2\, dr, \tag{70}$$

where $\hat{k}$ is a unit vector parallel to $\vec{k}$, j_n is the spherical Bessel function of order n, and primes denote differentiation with respect to r.

For several reasons, the most interesting of the various dynamical structure factors is the charge-fluctuation spectrum $S_{zz}(k,\omega)$. The linear response of the plasma to an external electric field can be described in terms of the charge-response function (or generalized susceptibility)

$$\chi_{zz}(k,\omega) = \chi'_{zz}(k,\omega) + i\chi''_{zz}(k,\omega), \tag{71}$$

which is related to $S_{zz}(k,\omega)$ through the fluctuation-dissipation theorem[20]

$$\chi_{zz}(k,\omega) = -\frac{1}{k_B T}\int_{-\infty}^{+\infty} \omega' S_{zz}(k,\omega')\times\left(P\frac{1}{\omega'-\omega} + i\pi\delta(\omega-\omega')\right)d\omega', \tag{72}$$

where P denotes the principal value. The wave-number and frequency-dependent dielectric function is expressible[18] in terms of the response function by

$$\frac{1}{\epsilon(k,\omega)} = 1 + \frac{k_D^2}{k^2}k_B T\chi_{zz}(k,\omega) \tag{73}$$

which generalizes the static result (27). Finally, the wave-number and frequency-dependent electrical conductivity $\sigma(k,\omega)$, which relates the induced electric-current density to the external electric field, can be determined[18] from a knowledge of the charge-fluctuation spectrum via the expression

$$\epsilon(k,\omega) = 1 - \frac{4\pi}{i\omega}\sigma(k,\omega). \tag{74}$$

In particular, the static conductivity σ introduced in the preceding section is the long-wavelength low-frequency limit of the real part of $\sigma(k,\omega)$, i.e.,

$$\sigma = \lim_{\omega\to 0}\lim_{k\to 0}\sigma'(k,\omega). \tag{75}$$

From Eqs. (72)–(74) it is clear that all wave-number and frequency-dependent electrical properties of a plasma in or near thermodynamic equilibrium can be determined from a knowledge of the equilibrium charge-fluctuation spectrum $S_{zz}(k,\omega)$. The latter quantity is directly measurable in the course of MD simulations. From the configurations generated in the MD runs detailed in Table I, we have computed the three partial density-density correlation functions $F_{\alpha\beta}(k,t)$ for wave numbers compatible with the periodic boundary conditions. In reduced units the latter are of the form

$$q = (6\pi^2/N)^{1/3}(n_1^2+n_2^2+n_3^2)^{1/2}, \tag{76}$$

where n_1, n_2, n_3 are integers, of which one at least is nonzero. For the size of the system simulated in our work ($N=125$ electrons or ions), the smallest accessible wave number is therefore $q_m = 0.780$. Results on $F_{\alpha\beta}(q,t)$ have been obtained for the five smallest possible values and for $q = 3q_m = 2.340$; numerical Fourier transformation is then used to determine the three dynamical structure factors and hence the linear combinations (62)–(64).

Results for $S_{zz}(q,\omega)$ at the four smallest wave numbers are shown in Fig. 6 for the case $\Gamma = 0.5$, $r_S = 0.4$, in Fig. 7 for $\Gamma = 0.5$, $r_S = 1$, and in Fig. 8 for $\Gamma = 2$, $r_S = 1$; the zero-frequency values, $S_{zz}(q,\omega=0)$ are listed in Table IV. Examination of the spectra reveals a general pattern. In all cases there are two rather well-separated components; a sharp low-frequency (or "central") peak linked to the slow ionic motions, and a broad peak, or shoulder, at frequencies of the order of ω_{pe}, which is clearly a manifestation of the much faster electronic motions. In fact, in the high-frequency range, $S_{zz}(q,\omega)$ is almost entirely determined by $S_{ee}(q,\omega)$ alone, the contributions from $S_{ii}(q,\omega)$ and $S_{ie}(q,\omega)$ having practically disappeared. The main difference between $S_{zz}(q,\omega)$ and $S_{ee}(k,\omega)$ is the presence in the latter of a

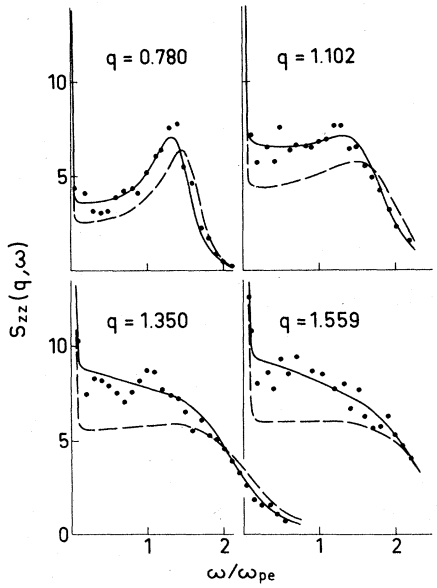

FIG. 6. Spectrum of charge-density fluctuations (multiplied by 100) for $\Gamma = 0.5$, $r_S = 0.4$ and four values of q. Dots: MD results. Full curves: Calculated from memory-function theory described in text. Dash curves: Vlasov theory.

central peak which is considerably more pronounced than in the former. This difference is particularly noticeable at small q; a detailed comparison is made in Fig. 3 of Ref. 6.

The high-frequency peak in $S_{ee}(q, \omega)$ and $S_{zz}(q, \omega)$ represents a mode corresponding to a propagating charge fluctuation or, put more simply, a plasma oscillation. The damping of the propagating mode

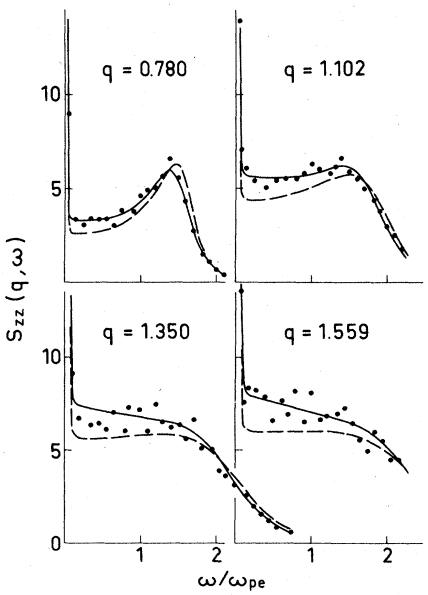

FIG. 7. Same as in Fig. 6, but for $\Gamma = 0.5$, $r_S = 1$.

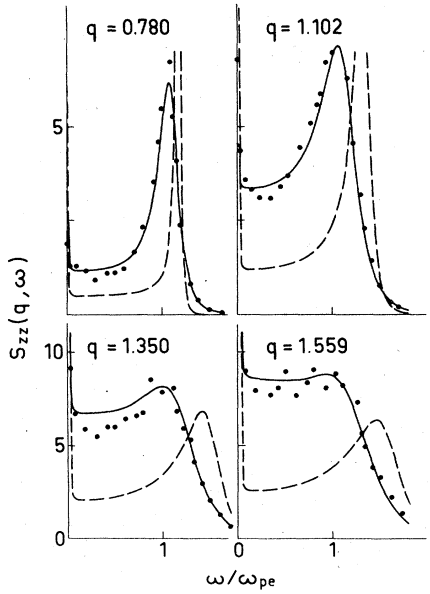

FIG. 8. Same as in Fig. 6, but for $\Gamma = 2$, $r_S = 1$.

increases rapidly with q. In fact, for the two high-temperature runs ($\Gamma = 0.5$, $r_S = 0.4$ and 1), the mode is well defined only at the smallest accessible wave number. In the case of stronger coupling ($\Gamma = 2$), the plasmon peak is considerably sharper and shifted to lower frequencies (see Fig. 8). The MD spectra shown in Figs. 6–8 are seen to differ significantly from the standard mean-field (Vlasov) results,[3] particularly in the strong coupling case. The failure of mean-field theory to reproduce the MD results reflects the importance of collisional damping; only at the largest wave number investigated (i.e., $q = 2.340$) are the predicted spectra everywhere in reasonable agreement with the MD results.

Before turning to a theoretical analysis of the data generated in the simulations, it is instructive to make a brief comparison with results obtained for related systems. In the OCP, one of the components is "smeared out" to form a uniform neutralizing background. Hence there is only one characteristic (plasma) frequency, the charge-fluctuation spectra exhibit no trace of a central peak,[13,25] and the high-frequency region of the spectrum (i.e., the plasmon peak) bears only a qualitative resemblance to that seen in the present calculations. A more detailed comparison (for the same value of the coupling constant) is made in Ref. 6. On the other hand, molten alkali halides are true two-component systems with some features in common with the hydrogen plasma. The most important differences are that the masses of the two components in the molten salt are of the same order of magnitude, and that under lab-

TABLE IV. Values of $S_{zz}(q, \omega=0)$. MD: molecular-dynamics results; mft: results of memory-function theory described in text; V = predictions of Vlasov theory.

	$\Gamma=0.5,\ r_S=0.4$ $S_{zz}(q,\omega=0)$			$\Gamma=0.5,\ r_S=1$ $S_{zz}(q,\omega=0)$			$\Gamma=2,\ r_S=1$ $S_{zz}(q,\omega=0)$		
q	MD	mft	V	MD	mft	V	MD	mft	V
0.780	0.26	0.32	0.39	0.33	0.40	0.39	0.02	0.025	0.064
1.102	0.86	0.79	0.80	0.85	0.83	0.80	0.07	0.045	0.16
1.350	1.20	1.26	1.17	1.28	1.22	1.17	0.21	0.15	0.29
1.559	1.45	1.60	1.38	1.80	1.51	1.38	0.40	0.32	0.39
2.340	2.52	2.48	1.91	2.10	2.23	1.91	1.84	1.70	0.90

oratory conditions the coupling constant is much larger ($\Gamma \simeq 50$) than for the plasma. In earlier calculations[23] on a simple symmetric (equal-mass) model for molten salts, the charge-fluctuation spectrum was shown to have a rather strongly damped plasmon peak. Because of the strong coupling, the plasmon mode is found to persist to wave numbers which, in reduced units, are somewhat higher than in the plasma. The central peak, however, is broader and less pronounced in the molten salt calculations than it is in the present work, where it describes what has been termed an "interspecies momentum relaxation" mode.[26-28] It is clear that in molten salts there is no clear cut distinction between short- and long-time scales of the type found here.

It should be noted, finally, that the MD simulations so far undertaken do not yield reliable results for the mass-mass and mass-charge dynamical structure factors since, as shown by Eqs. (62) and (63), these are dominated by the slow ionic motions. However, the theoretical analysis sketched in Sec. VI does give some information concerning the slow modes of the system.

VI. THEORETICAL ANALYSIS

We have seen in the preceding section that Vlasov theory is inadequate for the description of the charge-fluctuation spectra obtained in the MD calculations. To this we should add that a rigorous kinetic theoretical analysis[27] shows that ion-electron collisions cause the plasmon mode to be damped and shifted even at long wavelengths. Such effects are neglected in the Vlasov treatment. Furthermore, since the Vlasov equation contains no collision term, the spectrum at a particular wave number depends only on the coupling constant Γ, not on the parameter r_S; in fact, comparison of Figs. 6 and 7 reveals a weak but non-negligible dependence on r_S in the MD results.

To describe the results of the MD calculations, it is necessary to develop a strong coupling theory which takes proper account of static correlations and, in particular, of the coupling between the microscopic densities of ions and electrons. In doing so, we have adopted a Mori-Zwanzig memory-function approach of the type employed by Abramo *et al.*[29] for the analysis of collective motions in ionic liquids. By proceeding in this way, we obtain explicit expressions for the three partial dynamical structure factors $S_{\alpha\beta}(k, \omega)$, whereas Vlasov theory yields only the function $S_{ZZ}(k, \omega)$.

In view of the importance of ion-electron correlations, it is natural to attempt a description of the collective motions in the plasma in terms of the equation of motion of the two-component vector

$$|\vec{A}(t)\rangle = \begin{pmatrix} A_1(t) \\ A_2(t) \end{pmatrix} = \frac{1}{N^{1/2}} \begin{pmatrix} \rho^{(i)}(\vec{k}, t) \\ \rho^{(e)}(\vec{k}, t) \end{pmatrix}, \tag{77}$$

where the $\rho^{(\alpha)}(\vec{k}, t)$ are the Fourier components of the partial densities, defined by Eq. (55). However, it may be physically more appropriate to consider two independent linear combinations of the partial densities, such as the mass and charge densities introduced in Eqs. (58) and (59). Following Abramo *et al.*,[29] we define the following combinations, characterized by a single wave-number-dependent parameter $\theta(k)$:

$$\rho^{(1)}(\vec{k}, t) = M^{1/2}\rho^{(i)}(\vec{k}, t)\sin\theta(k) + \rho^{(e)}(\vec{k}, t)\cos\theta(k), \tag{78}$$

$$\rho^{(2)}(\vec{k}, t) = M^{1/2}\rho^{(i)}(\vec{k}, t)\cos\theta(k) - \rho^{(e)}(\vec{k}, t)\sin\theta(k), \tag{79}$$

where $M = m_i/m_e$. The choice of $\theta(k)$ will be specified later, but for certain values of $\theta(k)$ some simple relations are obtained. Thus,

$$\theta(k) = \tfrac{1}{2}\pi\colon\ \rho^{(1)}(\vec{k}, t) = M^{1/2}\rho^{(i)}(\vec{k}, t), \quad \rho^{(2)}(\vec{k}, t) = -\rho^{(e)}(\vec{k}, t), \tag{80}$$

and

$\theta(k)=\sin^{-1}\left(\frac{M}{M+1}\right)^{1/2}$:

$$\rho^{(1)}(\vec{k},t)=\left(\frac{1}{M+1}\right)^{1/2}\rho^{M}(\vec{k},t),$$
$$\rho^{(2)}(\vec{k},t)=\left(\frac{M}{M+1}\right)^{1/2}\rho^{Z}(\vec{k},t). \tag{81}$$

We now consider the description of the dynamical properties of the system which results from choosing for the components of $|\vec{\tilde{A}}(t)\rangle\rangle$ the linear combinations defined by (78) and (79). The information we require is contained in the 2×2 correlation function matrix defined as

$$\vec{\tilde{F}}(k,t)=\langle\vec{\tilde{A}}(t)\cdot\vec{\tilde{A}}^{*}(0)\rangle, \tag{82}$$

with elements $(a,b=1,2)$:

$$F_{ab}(k,t)=\langle A_a(t)A_b^{*}(0)\rangle$$
$$=\frac{1}{N}\langle\rho^{(a)}(\vec{k},t)\rho^{(b)}(-\vec{k},0)\rangle, \tag{83}$$

the Fourier-Laplace and Fourier transforms of which are given, respectively, by

$$\tilde{F}_{ab}(k,z)=\int_0^{\infty}e^{izt}F_{ab}(k,t)\,dt \tag{84}$$

and

$$\hat{F}_{ab}(k,\omega)=\frac{1}{2\pi}\int_{-\infty}^{\infty}e^{i\omega t}F_{ab}(k,t)\,dt$$
$$=\frac{1}{\pi}\tilde{F}'_{ab}(k,z=\omega). \tag{85}$$

From the spectral representation

$$\tilde{F}_{ab}(k,z)=i\int_{-\infty}^{\infty}\frac{\hat{F}_{ab}(k,\omega)}{z-\omega}d\omega, \tag{86}$$

it is straightforward to derive the high-frequency expansion of $\tilde{F}_{ab}(k,z)$ in terms of the frequency moments of $\hat{F}_{ab}(k,\omega)$, viz.,

$$\tilde{F}_{ab}(k,z)=\frac{i}{z}\sum_{n=0}^{i}\frac{\Omega_{ab}^{(2n)}(k)}{z^{2n}}. \tag{87}$$

The elements of the frequency-moment matrices $\vec{\tilde{\Omega}}^{(2n)}(k)$ are linear combinations of the moments $\Omega_{\alpha\beta}^{(2n)}$, the first three of which are given explicitly by Eqs. (66)–(68). Note that the form of Eqs. (78) and (79) means that

$$\Omega_{12}^{(2)}(k)=\Omega_{21}^{(2)}(k)=0, \tag{88}$$

i.e., the second frequency-moment matrix is diagonal for any choice of $\theta(k)$.

The correlation function matrix satisfies a generalized Langevin equation[5] of the form

$$[\vec{\tilde{M}}^{(1)}(k,z)-iz]\vec{\tilde{F}}(k,z)=\vec{\tilde{F}}(k,t=0), \tag{89}$$

where $\vec{\tilde{M}}^{(1)}(k,z)$ is a first-order memory-function matrix. Writing the latter as

$$\vec{\tilde{M}}^{(1)}(k,z)=\vec{\tilde{m}}^{(1)}(k,z)\cdot[\vec{\tilde{F}}(k,t=0)]^{-1}, \tag{90}$$

it follows from Eq. (87) that the high-frequency expansion of $\vec{\tilde{m}}^{(1)}(k,z)$ is given by

$$\vec{\tilde{m}}^{(1)}(k,z)=\frac{i}{z}[\vec{\tilde{\mu}}^{(0)}(k)+z^{-2}\vec{\tilde{\mu}}^{(2)}(k)+O(z^{-4})] \tag{91}$$

with

$$\vec{\tilde{\mu}}^{(0)}(k)=\vec{\tilde{\Omega}}^{(2)}(k)=\langle\dot{A}\dot{A}^{*}\rangle, \tag{92}$$
$$\vec{\tilde{\mu}}^{(2)}(k)=\vec{\tilde{\Omega}}^{(4)}(k)-\vec{\tilde{\Omega}}^{(2)}(k)[\vec{\tilde{\Omega}}^{(2)}(k)]^{-1}\vec{\tilde{\Omega}}^{(2)}(k). \tag{93}$$

The matrix elements of $\vec{\tilde{\mu}}^{(2)}(k)$ are

$$\mu_{11}^{(2)}(k)=\Omega_{11}^{(4)}(k)-\frac{1}{\Delta(k)}\Omega_{22}^{(0)}(k)[\Omega_{11}^{(2)}(k)]^2, \tag{94}$$

$$\mu_{12}^{(2)}(k)=\mu_{21}^{(2)}(k)$$
$$=\Omega_{12}^{(4)}(k)+\frac{1}{\Delta(k)}\Omega_{12}^{(0)}(k)\Omega_{11}^{(2)}(k)\Omega_{22}^{(2)}(k), \tag{95}$$

$$\mu_{22}^{(2)}(k)=\Omega_{22}^{(4)}(k)-\frac{1}{\Delta(k)}\Omega_{11}^{(0)}(k)[\Omega_{22}^{(2)}(k)]^2, \tag{96}$$

where

$$\Delta(k)=\Omega_{11}^{(0)}(k)\Omega_{22}^{(0)}(k)-[\Omega_{12}^{(0)}(k)]^2$$
$$=M\{S_{ii}(k)S_{ee}(k)-[S_{ie}(k)]^2\}. \tag{97}$$

In obtaining these results, use has been made of Eq. (88).

The memory-function hierarchy can be truncated at first order by making a simple ansatz for $m_{ab}^{(1)}(k,t)$. As an example, we could write the memory functions in Gaussian form, i.e., as

$$m_{ab}^{(1)}(k,t)=m_{ab}^{(1)}(k,t=0)\exp\{-[t/\tau_{ab}(k)]^2\}$$
$$=\mu_{ab}^{(0)}(k)\exp\{-[t/\tau_{ab}(k)]^2\} \tag{98}$$

and determine the three relaxation times $\tau_{11}(k)$, $\tau_{12}(k)[=\tau_{21}(k)]$, and $\tau_{22}(k)$ in terms of the quantities $\mu_{ab}^{(2)}$ by identifying the high-frequency expansion of (98) with the exact expansion given by Eq. (91). Such a procedure was in fact adopted for binary ionic mixtures (mixtures of OCP's) in Ref. 30. In the present case, the resulting charge-fluctuation spectra are in fair agreement with the MD results, but significant improvement can be achieved by passing to next order in the memory-function hierarchy. The second equation in the hierarchy relates the first-order memory-function matrix to a second-order matrix $\vec{\tilde{M}}^{(2)}(k,z)$ in a form analogous to (89), i.e.,

$$[\vec{\tilde{M}}^{(2)}(k,z)-iz]\vec{\tilde{M}}^{(1)}(k,z)=\vec{\tilde{M}}^{(1)}(k,t=0) \tag{99}$$

or

$$[\tilde{\tilde{M}}^{(2)}(k,z) - iz]\tilde{\tilde{m}}^{(1)}(k,z) = \tilde{\tilde{m}}^{(1)}(k,t=0). \quad (100)$$

The normalized second-order memory-function matrix is defined by the equation [cf. Eq. (90)],

$$\tilde{\tilde{M}}^{(2)}(k,z) = \tilde{\tilde{m}}^{(2)}(k,z) \cdot [\tilde{\tilde{m}}^{(1)}(k,t=0)]^{-1} \quad (101)$$

and has a high-frequency expansion starting as

$$\tilde{\tilde{m}}^{(2)}(k,z) = \frac{i}{z}[\tilde{\tilde{\mu}}^{(2)}(k) + O(z^{-2})]. \quad (102)$$

This result follows from Eqs. (91) and (100); the matrix elements of $\tilde{\tilde{\mu}}^{(2)}(k)$ are given explicitly by Eqs. (94)–(97).

We now proceed by making an exponential or Gaussian approximation for $m_{ab}^{(2)}(k,t)$ on writing either

$$m_{ab}^{(2)}(k,t) = \mu_{ab}^{(2)}(k)\exp[-t/\tau_{ab}(k)] \quad (103)$$

or

$$m_{ab}^{(2)}(k,t) = \mu_{ab}^{(2)}(k)\exp\{-[t/\tau_{ab}(k)]^2\}. \quad (104)$$

Adopting the approach of Abramo *et al.*,[29] we choose the disposable "mixing parameter" $\theta(k)$ so as to diagonalize the matrix $\tilde{\tilde{\mu}}^{(2)}(k)$; this has the effect of diagonalizing $\tilde{\tilde{m}}^{(2)}(k,z)$ within either of the approximations represented by Eqs. (103) and (104). If follows that the resulting dynamical structure factors will depend, for a given wave number, on only *two* independent relaxation times $\tau_{11}(k)$ and $\tau_{22}(k)$. From Eq. (95) we see that the condition for diagonalization is

$$\Omega_{12}^{(0)}(k)\Omega_{11}^{(2)}(k)\Omega_{22}^{(2)}(k) = -\Delta(k)\Omega_{12}^{(4)}(k). \quad (105)$$

This leads immediately to an equation for $\tan\theta(k)$ in the form

$$\tan^2\theta(k) + \phi(k)\tan\theta(k) - 1 = 0, \quad (106)$$

where

$$\phi(k) = \frac{\Delta(k)\Omega_{ee}^{(4)}(k) + S_{ee}(k)[\Omega_{ee}^{(2)}(k)]^2 - M\{\Delta(k)\Omega_{ii}^{(4)}(k) + S_{ii}(k)[\Omega_{ee}^{(2)}(k)]^2\}}{M^{1/2}\{\Delta(k)\Omega_{ie}^{(4)}(k) + S_{ie}(k)[\Omega_{ee}^{(2)}(k)]^2\}}. \quad (107)$$

From the known limits for small and large k of the various static quantities appearing in Eq. (107), it is easily shown that

$$\lim_{k\to 0}\tan\theta(k) = M^{1/2}, \quad (108)$$

$$\lim_{k\to\infty}\tan\theta(k) = \infty. \quad (109)$$

By comparing these results with those contained in (80) and (81) we find that in the long-wavelength limit the linear combinations $\rho^{(1)}(\vec{k},t)$ and $\rho^{(2)}(\vec{k},t)$ reduce (apart from constant factors) to the mass and charge densities (58) and (59), whereas in the limit $k\to\infty$ they reduce to the partial densities defined by Eq. (55). From a physical point of view, this limiting behavior is very satisfactory. In the limit $k\to 0$ we expect the dynamical behavior to be dominated by two well-defined longitudinal modes linked to mass and charge fluctuations, i.e., a sound-wave mode and a plasmon mode. On the other hand, the limit $k\to\infty$ corresponds to ideal-gas behavior, and the particles are expected to move independently; the approach to the ideal-gas limit necessarily involves a decoupling of fluctuations in the densities of the individual species.

We are left finally with the problem of determining the two relaxation times $\tau_{11}(k)$ and $\tau_{22}(k)$. Here again we follow the same lines as Abramo *et al.*,[29] adopting a prescription suggested earlier by Lovesey[31]; $\tau_{aa}(k)$ $(a=1,2)$ is calculated from the characteristic squared frequencies $\Omega_{aa}^{(4)}(k)/\Omega_{aa}^{(2)}(k)$ and $\Omega_{aa}^{(2)}(k)/\Omega_{aa}^{(0)}(k)$ by imposing the requirement that for $k\to\infty$ the resulting values of the dynamical structure factors at zero frequency should reduce to their known independent particle limits, i.e.,

$$\lim_{k\to\infty}\hat{F}_{11}(k,\omega=0) = \lim_{k\to\infty}MS_{ii}(k,\omega=0) = \frac{M}{k}\left(\frac{m_i}{2\pi k_B T}\right)^{1/2}, \quad (110)$$

$$\lim_{k\to\infty}\hat{F}_{22}(k,\omega=0) = \lim_{k\to\infty}S_{ee}(k,\omega=0) = \frac{1}{k}\left(\frac{m_e}{2\pi k_B T}\right)^{1/2}. \quad (111)$$

The resulting expressions for the two relaxation times associated with the Gaussian memory functions (104) are

$$\tau_{11}(k) = \left(\frac{\Omega_{11}^{(4)}(k)}{\Omega_{11}^{(2)}(k)} - \frac{\Omega_{11}^{(2)}(k)\Omega_{22}^{(0)}(k)}{\Delta(k)}\right)^{-1/2}, \quad (112)$$

$$\tau_{22}(k) = \left(\frac{\Omega_{22}^{(4)}(k)}{\Omega_{22}^{(2)}(k)} - \frac{\Omega_{22}^{(2)}(k)\Omega_{11}^{(0)}(k)}{\Delta(k)}\right)^{-1/2}. \quad (113)$$

The corresponding relaxation times for the exponential memory functions differ from these only by a factor $(\pi/4)^{1/2}$.

To determine the long-wavelength behavior of the two relaxation times, it is necessary only to replace the quantities appearing on the right-hand side of (112) and (113) by their limiting values for $k\to 0$. In this way it it easy to show $\tau_{11}(k)$ diverges as $k\to 0$, but that $\tau_{22}(k)$ remains finite. Since in the small-k limit, $\rho^{(1)}(\vec{k},t)$ and $\rho^{(2)}(\vec{k},t)$ go over,

TABLE V. Values of the frequency moments and relaxation times appearing in the memory-function analysis described in the text. All results are based on HNC calculations for potential model defined by Eq. (14). Starred quantities are in units in which $\omega_{pe}=1$.

q	S_{ii}	S_{ie}	S_{ee}	$\Omega_{ii}^{(4)}*$	$-\Omega_{ie}^{(4)}*$	$\Omega_{ee}^{(4)}*$	τ_{11}^{*}	τ_{22}^{*}
				(a) $\Gamma=0.5$, $r_S=0.4$				
0.307	0.5461	0.5235	0.5630	$0.2364E-07$	$0.3646E-04$	$0.7759E-01$	101.1	2.18
0.767	0.5803	0.4386	0.6590	$0.2607E-06$	$0.2092E-03$	0.8104	45.8	1.07
1.074	0.6256	0.3600	0.7390	$0.7651E-06$	$0.3765E-03$	$0.2360E+01$	33.4	0.785
1.381	0.6823	0.2813	0.8117	$0.1825E-05$	$0.5626E-05$	$0.5665E-01$	26.2	0.616
1.534	0.7117	0.2454	0.8424	$0.2665E-05$	$0.6578E-03$	$0.8314E+01$	23.7	0.556
2.301	0.8368	0.1185	0.9386	$0.1209E-04$	$0.1109E-02$	$0.3879E+02$	15.9	0.374
				(b) $\Gamma=0.5$, $r_S=1$				
0.307	0.5620	0.5344	0.5681	$0.2593E-07$	$0.4103E-04$	$0.8659E-01$	93.9	1.73
0.767	0.6159	0.4608	0.6468	$0.2751E-06$	$0.2487E-03$	0.8985	43.6	1.00
1.074	0.6662	0.3944	0.7142	$0.7936E-06$	$0.4729E-03$	$0.2574E+01$	32.4	0.756
1.381	0.7191	0.3270	0.7790	$0.1873E-05$	$0.7521E-03$	$0.6066E+01$	25.7	0.602
1.534	0.7447	0.2952	0.8080	$0.2724E-05$	$0.9085E-03$	$0.8828E+01$	23.3	0.546
2.301	0.8494	0.1709	0.9106	$0.1223E-04$	$0.1797E-02$	$0.3997E+02$	15.8	0.370
				(c) $\Gamma=2$, $r_S=1$				
0.307	0.7033	0.7130	0.7393	$0.5514E-08$	$0.9507E-05$	$0.1776E-01$	170.08	2.40
0.767	0.5638	0.5816	0.7191	$0.4100E-07$	$0.5243E-04$	0.1137	77.3	1.73
1.074	0.5131	0.5000	0.7382	$0.9521E-07$	$0.9124E-04$	0.2480	58.4	1.38
1.381	0.5065	0.4274	0.7766	$0.1902E-06$	$0.1320E-03$	0.4897	47.1	1.13
1.534	0.5171	0.3937	0.7989	$0.2588E-06$	$0.1522E-03$	0.6721	42.9	1.04
2.301	0.6493	0.2495	0.8987	$0.9414E-06$	$0.2461E-03$	$0.2659E+01$	29.8	0.72

respectively, to the microscopic densities of mass and charge, these results reflect the fact that the sound-wave mode becomes overdamped in the limit $k\to 0$, whereas the plasmon mode is not a genuine hydrodynamic mode but rather a "relaxation" mode[27,28] with a lifetime which remains finite even in the long-wavelength limit. For intermediate and large wave numbers ($q \gtrsim 1$), we find as expected, that $\tau_{11}(k)/\tau_{22}(k) \simeq M^{1/2}$.

The final expressions for the functions $\tilde{F}_{ab}(k,z)$ may be written as

$$\tilde{F}_{ab}(k,z)=\frac{1}{D(k,z)}[\Omega_{a2}^{(0)}(k)\Omega_{b2}^{(0)}(k)\tilde{m}_{11}^{(1)}(k,z) + \Omega_{1a}^{(0)}(k)\Omega_{1b}^{(0)}(k)\tilde{m}_{22}^{(1)}(k,z) - iz\,\Omega_{ab}^{(0)}(k)\Delta(k)], \tag{114}$$

with

$$D(k,z)=\tilde{m}_{11}^{(1)}(k,z)\tilde{m}_{22}^{(1)}(k,z)-\omega^2\Delta(k) - iz[\Omega_{11}^{(0)}(k)\tilde{m}_{22}^{(1)}(k,z)+\Omega_{22}^{(0)}(k)\tilde{m}_{11}^{(1)}(k,z)] \tag{115}$$

and

$$\tilde{m}_{aa}^{(1)}(k,z)=\frac{\Omega_{aa}^{(2)}(k)}{-iz+\tilde{m}_{aa}^{(2)}(k,z)/\Omega_{aa}^{(2)}(k)}, \tag{116}$$

where $\tilde{m}_{aa}^{(2)}(k,z)$ is the Fourier-Laplace transform of one of the two approximate memory functions (103) and (104). The corresponding dynamical structure factors $S_{ab}(k,\omega)[=\hat{F}_{ab}(k,\omega)]$ are obtained by taking the real part of $\tilde{F}_{ab}(k,z)$ [see Eq. (85)]. It is then straightforward to determine $S_{MM}(k,\omega)$, $S_{MZ}(k,\omega)$, and $S_{ZZ}(k,\omega)$ by inversion of the linear relations (78) and (79) and the use of Eqs. (62)–(64).

The static ingredients needed for the evaluation of Eqs. (114)–(116) are the frequency moments of zeroth, second, and fourth order. From Eqs. (66)–(68) we see that these quantities are entirely expressible in terms of the pair potentials and the pair distribution functions; the latter may be determined either from the simulations or, with high accuracy, by numerical solution of the coupled HNC equations (see Sec. III). Results obtained from HNC calculations for the nontrivial (i.e., zeroth- and fourth-) frequency moments and for the relaxation times $\tau_{11}(q)$ and $\tau_{22}(q)$ appropriate to the Gaussian memory functions (104) are listed in Table V for several values of q and the temperatures and densities corresponding to the MD simulations. (For technical reasons, the theoretical expressions have been evaluated for wave numbers which differ slightly from those studied in the MD calculations.) The resulting charge-fluctuation spectra are plotted in Figs.

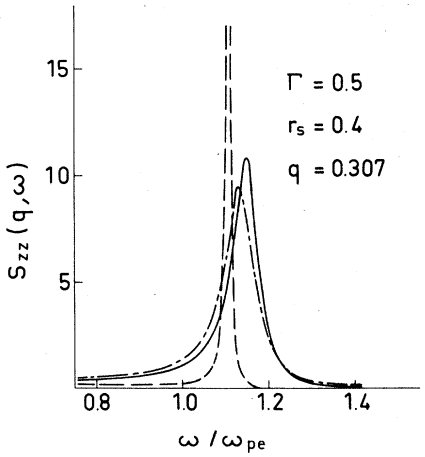

FIG. 9. Spectrum of charge-density fluctuations (multiplied by 100) for $\Gamma = 0.5$, $r_S = 0.4$ and $q = 0.307$. Full curve: Calculated from memory-function theory described in text and based on potential model defined by Eq. (14). Dot-dash curve: The same, but incorporating the electron symmetry term, defined by Eq. (16). Dash curve: Vlasov theory.

6–8 for comparison with the MD results. Although the comparison is complicated by the scatter in the "experimental" data, the agreement is clearly very good. If the exponential memory functions (103) are used, the good agreement is partly spoiled; the subsequent discussion is therefore limited to the Gaussian approximation represented by Eq. (104). The theory also yields results for the other dynamical structure factors, including $S_{MM}(q, \omega)$ and $S_{MZ}(q, \omega)$. These latter functions have an uninteresting structure, consisting solely of a central peak which broadens steadily with increasing q.

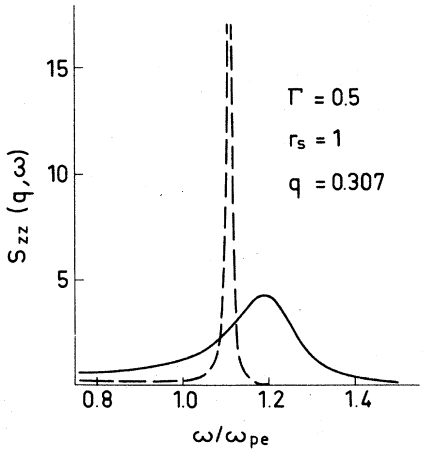

FIG. 10. Same as in Fig. 9, but for $\Gamma = 0.5$, $r_S = 1$. The effect of electron symmetry is negligible in this case.

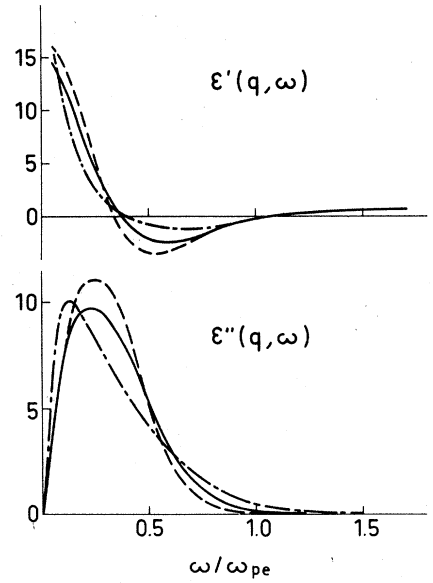

FIG. 11. Real (above) and imaginary (below) parts of the complex dielectric function for $\Gamma = 0.5$, $q = 0.307$. Dash curves: Vlasov theory. Other curves: Results of memory-function theory described in text for $r_S = 0.4$ (full) and $r_S = 1$ (dash-dot). Memory-function results are based on the potential model which incorporates electron symmetry, defined in Eq. (16).

Since the spectra predicted by the memory-function scheme are in such good agreement with the results of the simulations, it seems natural to use the same theoretical approach to obtain information on the collective dynamical modes in situations for which there are, as yet, no MD results available. Of particular interest is the behavior of the charge-fluctuation mode at long wavelengths. Accordingly, in Figs. 9–12, we show results obtained at $q = 0.307$ both for $S_{zz}(q, \omega)$ and for $\epsilon(q, \omega)$. The shortcomings of the Vlasov approximation which are already apparent at larger values of q (see Figs. 6–8) are even more strikingly evident here. The comparison made for $\epsilon(q, \omega)$ (Figs. 11–13) is particularly instructive, since it reveals that mean-field theory can yield results which are qualitatively incorrect, even at relatively large values of q (Fig. 13). When $q \ll ak_D$, collisionless (Landau) damping is negligible, and in the high-frequency region the Vlasov spectrum reduces to a near delta-function form centered close to ω_p. Examination of Figs. 9 and 10 shows that collisional damping has not only the obvious effect of broadening the plasmon peak, particularly at the lower density, but also that of shifting it to higher frequencies. At larger q, however, the shift is negative. The situation is summarized in Fig. 14, where the dispersion of the plasmon peak is plotted for the three thermo-

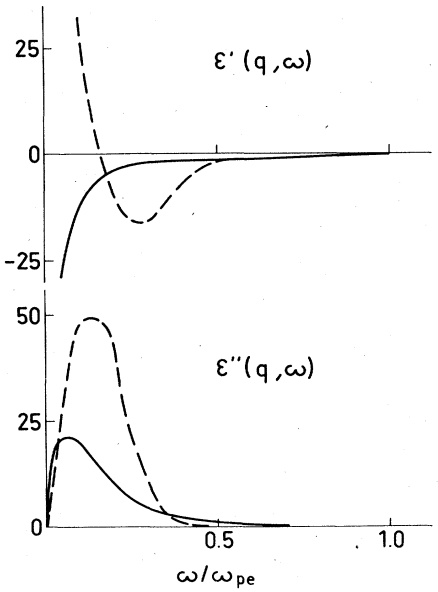

FIG. 12. Real (above) and imaginary (below) parts of the complex dielectric function for $\Gamma = 2$, $r_s = 1$ and $q = 0.307$. Full curves: Calculated from memory-function theory described in text for potential model which incorporates electron symmetry, defined by Eq. (16). Dash curves: Vlasov theory.

dynamic states for which MD calculations have been made. In each case, the plasmon mode at infinite wavelength is shifted to a frequency lying *above* ω_p. For a given coupling constant, the magnitude of the shift is quite sensitive to the value of r_s, but there is qualitative agreement, at least for $\Gamma = 0.5$, with a weak coupling calculation due to Baus.[28]

One factor that we have ignored so far is the effect of electron symmetry on the collective

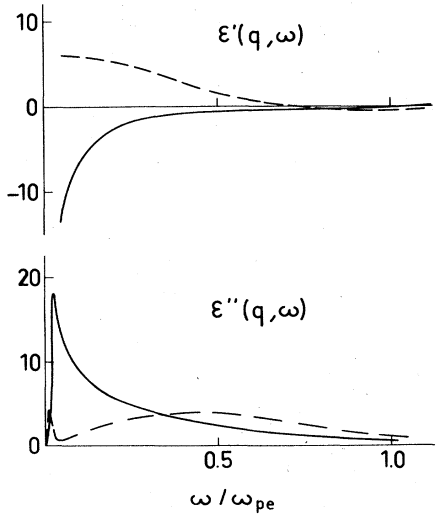

FIG. 13. Same as in Fig. 12, but for $q = 1.074$.

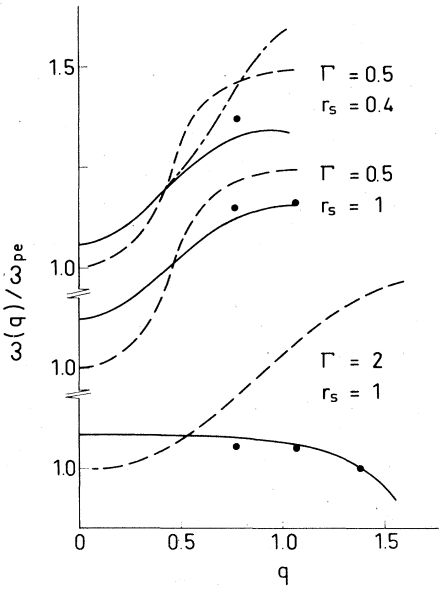

FIG. 14. Plasma dispersion curves as measured from the position of the high-frequency peak in $S_{zz}(q,\omega)$ for $\Gamma = 0.5$, $r_s = 0.4$ (above); $\Gamma = 0.5$, $r_s = 1$ (center), and $\Gamma = 2$, $r_s = 1$ (below). Dots: MD results. Full curves: Calculated from memory-function theory described in text. Dash curves: Vlasov theory. The dash-dot curve for $\Gamma = 0.5$, $r_s = 0.4$ shows the effect of electron symmetry as calculated from memory-function theory.

dynamics of the plasma. Since the charge fluctuations are dominated by the long range of the Coulomb potential, we do not expect electron symmetry to make a major contribution to $S_{zz}(q, \omega)$, notwithstanding its importance for static properties (see Sec. III). As a check, however, we have repeated the memory-function calculations with the frequency moments based on the potential model (16). Results obtained for $S_{zz}(q, \omega)$ at $q = 0.307$ and $\Gamma = 0.5$, $r_s = 0.4$ are plotted in Fig. 9. The effect is small, but increases with increasing q, the extra repulsion in the electron-electron interaction causing a shift of the plasmon peak to higher frequencies; dispersion curves computed with and without electron symmetry are compared in Fig. 14. At $\Gamma = 2$, which is close to the electron degeneracy limit, the effect not surprisingly, is more pronounced, but at a ten times higher temperature ($\Gamma = 0.2$) it is everywhere completely negligible.

Finally, we have made a preliminary study of the influence on the charge-fluctuation spectrum of changes in the mass ratio M by extending the memory-function calculations to the somewhat extreme case of a hypothetical plasma made up of protons and muons, for which $M \simeq 8.88$. Results obtained for both electron and muon plasmas at the same values of Γ and r_s are shown in Fig.

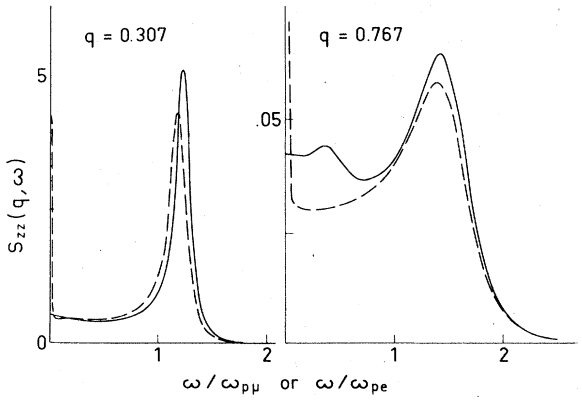

FIG. 15. Spectrum of charge-density fluctuations (multiplied by 100) for muon (full curves) and electron (dash curves) plasmas at $\Gamma = 0.5$, $r_s = 1$ and two values of q.

15. [Note that in absolute units the temperature of the muon plasma would be about 207 ($\simeq 1836/8.88$) times higher than in the electron plasma and the density would be approximately $(207)^3$ times greater.] The main difference between the two is the absence of an intense central peak in the case of the muon plasma, though there is a weak low-frequency peak at $q = 0.767$ which is clearly linked to the motion of the protons. In other respects, the spectra are surprisingly similar.

VII. DISCUSSION

We have shown that MD calculations on a semiclassical model of a dense nondegenerate hydrogen plasma are technically feasible despite the large difference in time scales of the ionic and electronic motions. Our quantitative results may be summarized as follows. First, the static properties of the plasma are very well described by the relevant system of coupled HNC equations. Second, computation of the ion and electron self-diffusion coefficients and of the electrical conductivity shows that the latter considerably exceeds the sum of the two mobilities. Third, the spectra of charge fluctuations and the complex dielectric function differ significantly from the predictions of Vlasov theory, particularly at small wave numbers, but the MD data are reproduced essentially exactly by a simple theoretical scheme which takes explicit account of ion-electron correlations. The only input information that the theory requires are the first three nonvanishing frequency moments of the partial dynamical structure factors, quantities which are easily obtained by HNC calculations; there are no adjustable parameters. This makes it possible to study, in an economical way, the dependence of the collective modes of the plasma on the precise form of the effective pair potentials.

One weakness of the theoretical model developed in Sec. VI is that it does not go over correctly to the Vlasov result in the limit $\Gamma \to 0$. This situation can be remedied, however, by applying the memory-function formalism to the response functions (susceptibilities) rather than to the correlation functions.[32] Work in that direction is in progress. Other projects in hand include the computation of other transport coefficients, including the thermal conductivity, and the extension of the simulations to include the important *nonequilibrium* situation in which the temperature of the electrons greatly exceeds that of the ions. It is worth adding, finally, that a MD investigation of the collective modes at significantly smaller wave numbers would be a useful undertaking. Although this would require the simulation of a much larger ($N \sim 10^3$) system, such a calculation seems very well suited to a vector processing machine.

ACKNOWLEDGMENTS

The authors acknowledge useful and stimulating discussions with M. Baus, C. Deutsch, H. Minoo, and L. Sjögren. Some of the calculations were carried out when one of us (I. R. M.) was at Royal Holloway College and we are grateful for the facilities provided by Professor K. Singer.

[1]See, e.g., *Strongly Coupled Plasmas*, edited by G. Kalman (Plenum, New York, 1978).
[2]See, e.g., Proceedings of the 20th Scottish Universities Summer School in Physics 1979, edited by J. J. Sanderson and R. A. Cairns (unpublished).
[3]S. Ichimaru, *Basic Principles of Plasma Physics* (Benjamin, Reading, 1973).
[4]M. Baus and J. P. Hansen, Phys. Rep. 59, 1 (1980).
[5]J. P. Hansen and I. R. McDonald, *Theory of Simple Liquids* (Academic, London, 1976).
[6]J. P. Hansen and I. R. McDonald, Phys. Rev. Lett. 41, 1379 (1978).
[7]See, e.g., the excellent review by E. L. Lieb, Rev. Mod. Phys. 48, 553 (1976).
[8]T. Dunn and A. A. Broyles, Phys. Rev. 157, 156 (1967); M. A. Pokrant, A. A. Broyles, and T. Dunn, Phys. Rev. A 10, 379 (1974).
[9]A. A. Barker, J. Chem. Phys. 55, 1751 (1971).
[10]C. Deutsch, Phys. Lett. 60A, 317 (1977).
[11]C. Deutsch, M. M. Gombert, and H. Minoo, Phys. Lett.

66A, 381 (1978); 72A, 481 (1979); C. Deutsch, M. M. Gombert, and H. Minoo (unpublished).
[12]F. J. Rogers, in Ref. 1.
[13]J. P. Hansen, I. R. McDonald, and E. L. Pollock, Phys. Rev. A 11, 1025 (1975).
[14]B. Bernu and P. Vieillefosse, Phys. Rev. A 18, 2345 (1978).
[15]I. R. McDonald, P. Vieillefosse, and J. P. Hansen, Phys. Rev. Lett. 39, 271 (1977).
[16]S. G. Brush, H. L. Sahlin, and E. Teller, J. Chem. Phys. 45, 2102 (1966).
[17]See, e.g., *Methods in Computational Physics*, edited by B. J. Alder, S. Fernbach, and M. Rotenberg (Academic, New York, 1970), Vol. 9.
[18]See, e.g., N. H. March and M. P. Tosi, *Atomic Dynamics in Liquids* (Macmillan, London, 1976).
[19]F. H. Stillinger and R. A. Lovett, J. Chem. Phys. 49, 1991 (1968).
[20]R. Kubo, J. Phys. Soc. Jpn. 12, 570 (1957). See also the discussion in D. Pines and P. Nozières, *The Theory of Quantum Fluids* (Benjamin, New York, 1966).
[21]J. F. Springer, M. A. Pokrant, and F. A. Stevens, J. Chem. Phys. 61, 2680 (1974).
[22]K. C. Ng, J. Chem. Phys. 61, 2680 (1974).
[23]J. P. Hansen and I. R. McDonald, J. Phys. C 7, L384 (1974); Phys. Rev. A 11, 2111 (1975).
[24]L. Spitzer, *Physics of Fully Ionized Gases* (Wiley, New York, 1962).
[25]M. Baus, Physica (Utrecht) 79A, 377 (1975).
[26]P. Vieillefosse and J. P. Hansen, Phys. Rev. A 12, 1106 (1975).
[27]E. F. DuBois and V. Gilinsky, Phys. Rev. A133, 1308 (1964); A133, 1317 (1964); E. J. Linnebur and J. J. Duderstadt, Phys. Fluids 16, 665 (1973); M. Baus, Physica (Utrecht) 88A, 319 (1977); 88A, 336 (1977); 88A, 347 (1977).
[28]M. Baus, Phys. Rev. Lett. 40, 793 (1978).
[29]M. C. Abramo, M. Parrinello, and M. P. Tosi, J. Phys. C 7, 4201 (1974).
[30]J. P. Hansen, I. R. McDonald, and P. Vieillefosse, Phys. Rev. A 20, 2590 (1979).
[31]S. W. Lovesey, J. Phys. C 4, 3057 (1971).
[32]S. Takeno and F. Yoshida, Prog. Theor. Phys. (Kyoto) 60, 1304 (1978).